ORIGINAL PAPER

# Photophysical Properties of Novel Picrate Derivatives – Solvent Effect

**Jayaraman Jayabharathi · Venugopal Thanikachalam ·
Manoharan Padmavathy ·
Marimuthu Venkatesh Perumal**

**Abstract** H and $^{13}$C NMR spectra were recorded for some novel picrate derivatives derived from 3,3-dimethyl-2,6-diarylpiperidin-4-ones and 3-benzyl-2,6-diarylpiperidin-4-one. The photophysical properties of the picrate derivatives were studied in several solvents, which include a wide range of apolar, polar and protic media. The observed lower fluorescence quantum yield may be due to an increase in the non-radiative deactivation rate constant. This is attributed due to the presence of increased electrostatic interaction between N-protonated piperidone ring and picryl anion ring so that the picryl anion ring lies perpendicular to the plane of the N-protonated piperidone ring i.e., non co-planarity. Such a geometrical change in the excited state leads to an important Stokes shift, reducing the reabsorption and reemission effects in the detected emission in highly concentrated solutions. The higher fluorescence quantum yield of the picrate derivatives are observed in polar media.

**Keywords** Picrates · Catalan parameters · Aggregation · Marcus · Reichardt-Dimroth solvent function

## Introduction

The relative chemical shift orders of equatorial and axial protons are in the normal chair conformation of cyclohexane and its derivatives ($\delta_{eq} - \delta_{ax}$) is attributed to the magnetic anisotropic effect of the C-C single bonds. The influence of substituents on the chemical shift of protons attached to the adjacent

J. Jayabharathi (✉) · V. Thanikachalam · M. Padmavathy ·
M. V. Perumal
Department of Chemistry, Annamalai University,
Annamalainagar 608 002, Tamilnadu, India
e-mail: jtchalam2005@yahoo.co.in

carbon has been reported [1] that the equatorial substituent at β- or γ-positon cannot affected the $\delta_{eq} - \delta_{ax}$ significantly. However, a γ-axial substituent or β-axial substituent can decrease $\delta_{eq} - \delta_{ax}$ value significantly. The negative value is even reported in t(4)-hydroxy-3,3-dimethyl-r(2),c(6)-diphenyl-piperidine where axial hydrogen at C-5 experiences severe 1,3-diaxial interaction with axial methyl group at the γ-position [C(3)] and deshielding magnetic anisotropic effect of axial hydroxy group at the β-position [C(4)].

Several factors contribute to the best laser performance of pyrromethene with respect to rhodamine as laser dye [2]: (1) low triplet-triplet absorption capacity at the lasing spectral region, which reduces the losses in the resonator cavity; (2) a poor tendency to self-aggregate in organic solvents, avoiding the fluorescence quenching of the monomer emission by the presence of aggregates in highly concentrated solutions, as observed in rhodamine dyes: (3) and their high photo-stability, [3–5] which improves the lifetime of the laser action with respect to that of rhodamines [6]. Owing to these properties, PM dyes have been successfully incorporated into different solid matrixes (polymers, silica, etc.,) [7–9] to develop solid-state syntonizable dye lasers.

Photophysical properties and laser characteristics of compounds in liquid solutions and in polymeric matrixes, [7, 9] indicating that the laser behaviour is a consequence of the photophysical properties. Indeed, the evolution of the fluorescence wavelength and quantum yield with several environmental factors was similar to that observed for the laser band and efficiency, respectively. The Stokes shift modifies the lasing performance [10] in highly concentrated solutions because it affects the reabsorption and reemission phenomena, which shifts the emission band to longer wavelength and reduces its efficiency. In the present paper, the photophysical properties of the picrate derivatives (**1–4**) were investigated in a wide variety of solvents, including apolar, polar and protic

solvents. The solvent effects on the absorption and fluorescence bands were analyzed by a multi-component linear regression in which several solvent parameters are simultaneously analyzed. The fluorescence quantum yield and the Stokes shift are analyzed to look for the best conditions to improve the optical efficiencies of these picrate derivatives.

## Experimental Section

### Materials and Methods

*General Procedure for the Synthesis of Picrate Derivatives (1–4)*

3,3-dimethyl- and 3-benzyl-2,6-diarylpiperidin-4-ones were prepared as per literature procedure [11]. The piperidinium picrates (1–4) were prepared by mixing equimolar solution of piperidin-4-one in ethanol (0.01 M) with picric acid in ethanol (0.01 M) and the solution was stirred for 30 min at 27 °C. The yellow needles formed were recrystallized twice in benzene (Scheme 1).

*t(3,3)-Dimethyl-r(2),c(6)-bis-p-Methylphenylpiperidone Picrate (1)*
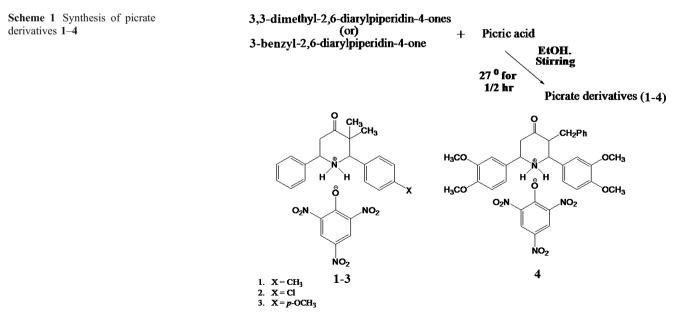
The piperidinium picrate t(3,3)-dimethyl-r(2),c(6)-bis-p-methylphenylpiperidone picrate (1) was prepared by mixing equimolar solution of t(3,3)-dimethyl-r(2),c(6)-bis-p-methylphenylpiperidin-4-one in ethanol (0.01 M) with picric acid in ethanol (0.01 M).The solution was stirred for 30 min at 27 °C. The yellow needles formed were recrystallized twice in benzene. Yield: 60%, d.p. 164 °C, $^1$H NMR: 4.75

H(6) (d, 10.0), 4.44 H(2) (s), 2.83 H(5e) (d, 14.5), 3.88 H(5a) (t), 1.49 CH$_3$ (eq) (s), 1.07 CH$_3$ (ax) (s), 2.26 PhCH$_2$ (d), 9.14 picryl proton (s), 7.07–7.05 aromatic *ortho* protons, 7.34–7.29 ppm (aromatic *meta* protons). $^{13}$C NMR: 71.33 C(2), 69.65 C(6), 48.84 C(3), 206.70 C(4), 40.01 C(5), 19.80 CH$_3$ (eq), 21.10 CH$_3$ (ax), 1.07 PhCH$_2$, 154.67 and 137.88 (ipso carbons), aromatic carbons: 129.77, 129.34, 128.90, 127.90, 127.82, 126.32.

*t(3,3)-Dimethyl-r(2),c(6)-bis- p-Chlorophenylpiperidone Picrate (2)*

The piperidinium picrate t(3,3)-dimethyl-r(2),c(6)-bis-p-chlorophenylpiperidone picrate (2) was prepared by mixing equimolar solution of t(3,3)-dimethyl-r(2),c(6)-bis-p-chlorophenylpiperidin-4-one in ethanol (0.01 M) with picric acid in ethanol (0.01 M).The solution was stirred for 30 min at 27 °C. The yellow needles formed were recrystallized twice in benzene. Yield: 70%, d.p. 196 °C, $^1$H NMR: 4.19 H(6) (s), 3.94 H(2) (s), 2.56 H(5e) (d, 11.05), 3.28 H(5a) (s), 1.26 CH$_3$ (eq) (s), 0.09 CH$_3$ (ax) (s), 9.22 picryl proton (s), 7.36–7.46 aromatic protons, 7.36–7.46 ppm aromatic *ortho* protons, 7.29–7.32 ppm (aromatic *meta* protons). $^{13}$C NMR: 63.77 C(2), 51.70 C(6), 44.58 C(3), 204.89 C(4), 35.57 C(5), 20.39 CH$_3$ (eq), 19.21 CH$_3$ (ax), 144.18 and 137.54 (ipso carbons), aromatic carbons: 160.77, 159.83, 156.98, 155.56, 154.37, 153.43.

*t(3,3)-Dimethyl-r(2),c(6)-bis-p-Methoxyphenyl Piperidone Picrate (3)*

The piperidinium picrate t(3,3)-dimethyl-r(2),c(6)-bis-p-methoxyphenylpiperidone picrate (3) was prepared by

**Scheme 1** Synthesis of picrate derivatives 1–4

mixing equimolar solution of t(3,3)-dimethyl-r(2),c(6)-bis-p-chlorophenylpiperidin-4-one in ethanol (0.01 M) with picric acid in ethanol (0.01 M).The solution was stirred for 30 min at 27 °C. The yellow needles formed were recrystallized twice in benzene. Yield: 65%, d.p. 158 °C, ^{1}H NMR: 4.69 H(6) (s), 4.42 H(2) (s), 2.81 H(5e) (d, 15.0), 3.25 H(5a) (d), 1.25 CH$_3$ (eq) (d), 1.07 CH$_3$ (ax) (s), 3.47 and 3.71 OCH$_3$ (d), 9.18 picryl proton (s), 6.78–6.80 aromatic *ortho* protons, 7.33–7.36 ppm aromatic *meta* protons. ^{13}C NMR: 63.86 C(2), 59.11 C(6), 49.05 C(3), 206.60 C(4), 39.99 C(5), 21.15 CH$_3$ (eq), 19.60 CH$_3$ (ax), 55.30 and 55.26 OCH$_3$, 137.61 and 130.27 (ipso carbons), aromatic carbons: 129.19–126.31.

### t(3)-Benzyl-r(2),c(6)-bis-3,4-Dimethoxyphenyl Piperidone Picrate (4)

The piperidinium picrate *t(3)-benzyl-r(2),c(6)-bis-3,4-dimethoxyphenyl piperidone picrate* (**4**) was prepared by mixing equimolar solution of *t*(3)-benzyl-r(2),c(6)-bis-3,4-dimethoxyphenylpiperidin-4-one in ethanol (0.01 M) with picric acid in ethanol (0.01 M).The solution was stirred for 30 min at 27 °C. The yellow needles formed were recrystallized twice in benzene. Yield: 70%, d.p. 140 °C, ^{1}H NMR: 4.00 H(6) (s), 3.79 H(2) (d, 12.10), 3.01 H(3) (s), 2.78 H$_{5e}$ (d, 13.30), 3.90 H$_{5a}$ (d), 3.56, 3.64 PhCH$_2$ (m), 3.91–3.94 OCH$_3$ (m), 9.20 picryl (s), aromatic protons: 6.59–7.50 ppm. ^{13}C NMR: 63.72 C(2), 61.61 C(6), 44.52 C(3), 204.89 C(4), 43.11 C(5), 30.52 PhCH$_2$, 55.92 (OCH$_3$), aromatic carbons: 137.81, 137.35, 129.32, 128.36, 128.31, 126.29.

UV–vis absorption and fluorescence spectra were recorded on Perkin Elmer spectrophotometer Lambda35 and Perkin Elmer LS55 spectrofluorimeter, respectively. Fluorescence spectra were corrected from the monochromator wavelength dependence and the photomultiplier sensibility. Fluorescence quantum yields (φ) have been determined by means of the corrected fluorescence spectra of a dilute solution of picrate derivatives in dichloromethane using coumarin as a reference and by taking into account the solvent refractive index. Radiative decay curves were recorded by means of a time-correlated single-photon counting technique. The time-resolved fluorescence spectra have been recorded using a HORIBA JOBIN YNON-SPEX F$_{13}$-111 Spectrofluorimeter available at Pondicherry University.
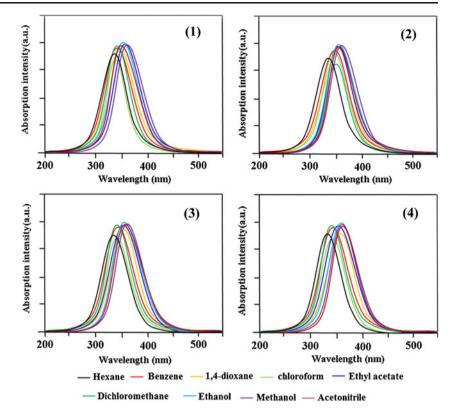
The photophysical properties of the picrate derivatives (**1**–**4**) were recorded in dilute concentrations ($1 \times 10^{-5}$ M). The fluorescence decay curves have been analyzed as mono exponentials ($\chi^2 < 1.2$), and the fluorescence decay time ($\tau$) was obtained from the slope. The rate constant for the radiative ($k_r$) and non-radiative ($k_{nr}$) deactivation pathways were calculated using these equations: $k_r = \Phi_p/\tau$, $k_{nr} = 1/\tau - \Phi_p/\tau$ and $\tau = (k_r + k_{nr})^{-1}$.

**Table 1** Photoluminescence spectral data of picrate derivatives **1**–**4**

| Solvent | Absorption[a] (λ, nm) | | | | Emission[b] (λ, nm) | | | | Stokes shift (cm$^{-1}$) | | | | 1 | | | | |
|---|---|---|---|---|---|---|---|---|---|---|---|---|---|---|---|---|---|
| | 1 | 2 | 3 | 4 | 1 | 2 | 3 | 4 | 1 | 2 | 3 | 4 | φ | τ (ns) | $k_r$ ($10^8$ s$^{-1}$) | $K_{nr}$ ($10^8$ s$^{-1}$) | |
| *n*-Hexane | 334 | 334 | 337 | 336 | 376 | 375 | 373 | 374 | 3344 | 3273 | 2864 | 3024 | 0.24 | 2.25 | 1.06 | 0.53 | |
| 1,4-dioxane | 346 | 355 | 354 | 360 | 402 | 404 | 406 | 404 | 4026 | 3417 | 3618 | 3025 | 0.21 | 2.27 | 0.93 | 0.54 | |
| Benzene | 341 | 348 | 344 | 345 | 393 | 383 | 382 | 385 | 3880 | 2626 | 2892 | 3011 | 0.13 | 1.81 | 0.72 | 0.55 | |
| Chloroform | 340 | 347 | 342 | 346 | 426 | 428 | 425 | 420 | 5938 | 5454 | 5710 | 5092 | 0.18 | 2.05 | 0.62 | 0.56 | |
| Ethyl acetate | 355 | 352 | 353 | 354 | 466 | 456 | 465 | 453 | 6710 | 6479 | 6823 | 6174 | 0.25 | 2.21 | 1.31 | 0.54 | |
| Dichloromethane | 344 | 349 | 347 | 348 | 414 | 403 | 410 | 406 | 4915 | 3839 | 4428 | 4105 | 0.16 | 2.59 | 1.14 | 0.54 | |
| Ethanol | 352 | 354 | 355 | 357 | 456 | 449 | 447 | 455 | 6479 | 5977 | 5798 | 6033 | 0.24 | 2.01 | 1.19 | 0.56 | |
| Methanol | 356 | 355 | 356 | 356 | 463 | 457 | 433 | 456 | 6492 | 6287 | 4995 | 6160 | 0.29 | 2.21 | 1.15 | 0.53 | |
| Acetonitrile | 349 | 352 | 354 | 356 | 454 | 461 | 448 | 459 | 6627 | 6717 | 5927 | 6303 | 0.25 | 2.17 | 1.11 | 0.54 | |

[a] UV–vis absorption measured in solution concentration = $1 \times 10^{-5}$ M
[b] Photoluminescence measured in solution concentration = $1 \times 10^{-4}$ M

Fig. 1 Absorption spectra of **1**–**4** in various solvents



Computational Details

Quantum mechanical calculations have been used to carry out the optimized geometry and HOMO-LUMO energies with Guassian-03 program using the Becke3-Lee-Yang-Parr (B3LYP) functional supplemented with the standard 6–31 G (d,p) basis set [12].

## Results and Discussion

Photophysical Properties of Picrate Derivatives (**1**–**4**) in Solution

Absorption and emission properties of these picrate derivatives (**1**–**4**) have been studied in various solvents. The absorption band maxima ($\lambda_{abs}$), emission band maxima ($\lambda_{emi}$) and the associated Stokes shift ($\upsilon_{ss}$) together with the fluorescence quantum yields for **1** ($\Phi_f$) are shown in Table 1.

Measurement of absorption solvatochromism (Fig. 1) have been interpreted with Marcus and Reichardt-Dimroth solvent functions to estimate the transition dipoles associated with low lying excited state. The linear correlation (Fig. 2) of solvent shift of absorption band position of these picrates (**1**–**4**) with Reichardt-Dimroth solvent $E_T$ parameters is indicative of the fact that the dielectric solute solvent interactions are responsible for the observed solvatochromic shift for the

picrates derivatives. The observed linear correlation (Fig. 3) of solvent shift of absorption band positions of these picrate derivatives (**1**–**4**) with Marcus optical dielectric solvent function $\left[ (1 - D_{op})/(2D_{op} + 1) \right]$ reveal that the transition dipoles associated with absorption and the direction of excited dipole is opposite to that of the ground state-dipole [13].

It is evident from Fig. 4 that the red shift of the maximum emission ($\lambda_{emi}$) may be due to the presence of increased electrostatic interaction between the N-protonated piperidone ring and the picryl anion ring so that the picrate anion ring lies perpendicular to the plane of the piperidone ring i.e., non co-planarity. Optimization of these picrate
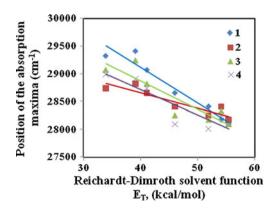


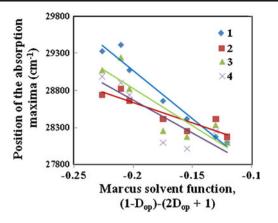Fig. 2 Reichardt-Dimroth solvent function vs position of the absorption maxima of **1**–**4**

Fig. 3 Marcus solvent function vs position of the absorption maxima of 1–4

derivatives (1–4), by DFT at B3LYP/6–31 G(d,p), have been performed using Gaussian-03. From the optimized structures (Fig. 5) it was found that there is poor co-planarity between the N-protonated piperidone ring and picryl anion ring. When the solution of picric acid is added to piperidone solution, protonation occurs at the nitrogen and additional axial N-H bond present in the protonated derivatives so that the nitrogen acquires positive charge. The bond distance between the $ax_{(N-H)}$.......$O^-$ is found to be higher in magnitude than $eq_{(N-H)}$......... $O^-$ (Table 2). The angle of tilting between the N-protonated piperidone ring and the picryl anion ring N18-C19-C1-C2 [41.6 (1), 84.6 (2), 88.9 (3) and 90.4 (4)] confirmed the non-coplanarity of the picrate derivatives and this may be the cause for the observed solvatochromic shifts.
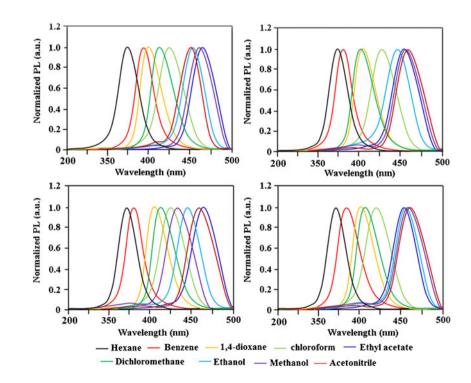
## Solvent Effects on the Absorption and Fluorescence Properties

All these picrate derivatives (1–4) show solvatochromism (Table 1) i.e., changes in the polarity of the solvents and charge transfer takes place. The position of the longer-wavelength absorption and emission bands in the spectra has been determined in several protic and aprotic solvents. Lippert-Mataga [14] plot (Fig. 6) have been constructed for the normal fluorescence spectrum of these picrate derivatives (1–4) using the following equation.

$$\bar{v}_{ss} = \bar{v}_{ab} - \bar{v}_{fl} = const + \left[\frac{2(\mu_e - \mu_g)^2}{hca^3}\right]f(D,n) \quad (1)$$

where $f(D,n) = (D-1)/(2D+1) - (n^2-1)/(2n^2+1)$, indicates the orientation polarizability and depicts polarity parameter of the solvent [15], $n$ is refractive index, D is dielectric constant, $\mu_e$ and $\mu_g$ are the dipole moments of the species in $S_1$ and $S_0$ states, respectively, $h$ is Planck's constant; $c$ is velocity of light and $a$ is Onsagar's cavity radius. The Lippert-Mataga plot is linear for the non-polar and polar/aprotic solvents with excellent correlation coefficient.

Large Stokes shifted fluorescence band suggests that this emission has originated from the species which is not present in the $S_0$ state and large geometrical change have takes place in the species when excited to $S_1$ state and the larger Stokes shift may be explained by the presence of electrostatic interaction between N-protonated piperidone
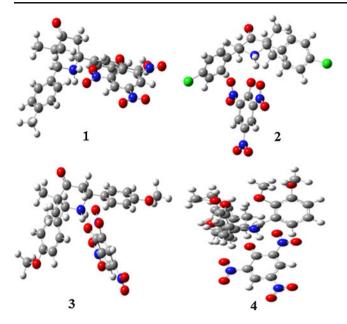
Fig. 4 Emission spectra of 1–4 in various solvents

Fig. 5 Molecular modeling of picrates 1–4



Fig. 6 Lippert-Mataga plot of 1–4

ring and the picryl anion ring with polar solvent molecules leading to the stabilization of the solvated isomers of these picrate derivatives (1–4).

The higher bathochromic shifts observed in the fluorescence band of the picrate derivatives can be interpreted by the Brunings-Corwin effect [16]. Because the distortion of the geometry in the excited state implies a decrease in the resonance energy, the fluorescence band is bathochromically shifted to a higher extent than the absorption band. Moreover, the loss of planarity in the excited state of these picrate derivatives could explain the lower fluorescence quantum yield in apolar solvents, owing to an increase in the non-radiative processes.

However, the shape of the absorption band is independent of the picrate concentration suggesting the poor aggregation and it is a suitable behaviour in the performance of active media of optics. Indeed, high concentration is necessary to bring about optic action, and the presence of aggregates drastically reduced the fluorescence quantum yield owing to the efficient quenching of the monomer fluorescence by the aggregates [17]. However, the experimental data indicate that the fluorescence band is shifted to
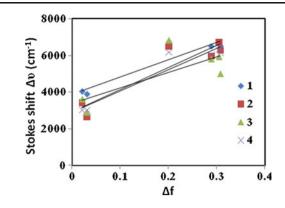
lower energies by increasing the concentration. This bathochromic shift is attributed to reabsorption and reemission phenomena [18] and this result corroborates the importance of registering photophysical properties in dilute solutions.

The HOMO-LUMO energy gap for these picrate derivatives (1–4) were calculated by B3LYP/6–31 G(d,p) and their HOMO-LUMO orbital pictures were given in Fig. 7. From the HOMO-LUMO orbital picture it was found that in compound 1 the filled $\pi$ orbital (HOMO) is located on the picryl anion ring, protonated nitrogen, C2 & C6 carbons and partly on the carbonyl oxygen and the unfilled $\pi^*$ orbital (LUMO) on the picryl anion ring. Whereas in compound 2 the filled $\pi$ orbital (HOMO) is located on the picryl anion ring and partly carbonyl oxygen and the unfilled $\pi^*$ orbital (LUMO) on the picryl anion ring and C2 & C6 carbons. In the case of compounds 3 and 4, the HOMO is located only on the picryl anion ring and the LUMO is located on the picryl anion ring (not on the picryl oxygen).The HOMO→LUMO transition implies that intramolecular charge transfer takes place within the molecule. The resonance structures of the picrate chromophores (Fig. 8) reveals that the resonance structure "b" has the largest charge separation along the short molecule axis. Since picryl anion ring is in $p$-quinanoid form which is energetically more stable when compared with other resonance structures. Consequently, its contribution would be more important in the $S_0$ ground state than in the $S_1$ excited state. Thus, the polar solvents would stabilize the $S_0$ state more extensively than the $S_1$ state, thereby increasing the energy gap between both states and explaining the solvatochromic shifts [19].

A multi-parameter correlation analysis [20, 21] is employed in which a physicochemical property is linearly correlated with several solvent parameters by means of Eq. 1:

$$(XYZ) = (XYZ)_0 + C_a A + C_b B + C_c C + \dots \qquad (2)$$

where $(XYZ)_0$ is the physicochemical property in an inert solvent and $C_a$, $C_b$, $C_c$ and the adjusted coefficients that

Table 2 Bond distances of axial and equatorial hydrogens with picryl oxygen 1–4

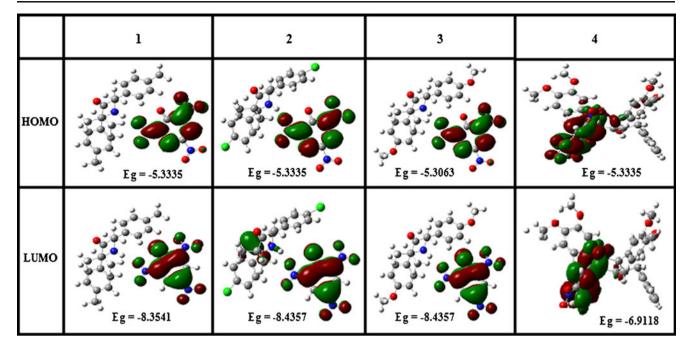| Compound | $d_{eqN-H}$-….O- (Å) | $d_{axN-H}$-….O- (Å) |
|---|---|---|
| 1 | 1.95 | 2.69 |
| 2 | 1.95 | 3.49 |
| 3 | 1.95 | 3.49 |
| 4 | 1.21 | 2.66 |

**Fig. 7** HOMO-LUMO orbital picture of **1**–**4**

reflect the dependence of the physicochemical property (XYZ) on several solvent properties. Solvent properties that mainly affect the photophysical properties of aromatic compounds are polarity, H-bond donor capacity and electron donor ability. Different scales for such parameters can be found in the literature. Taft et al., [22] propose the $\pi^*$, $\alpha$ and $\beta$ scales, whereas more recently Catalan et al., [23] suggest the $SPP^N$, SA and SB scales to describe the polarity/polarizability, the acidity and basicity of the solvents, respectively.

Figures 9a & b shows the obtained correlation between the absorption and fluorescence wavenumbers calculated by the multi-component linear regression by employing the Taft-proposed solvent parameters and the experimental values are given in Table 3. Table 3 lists the obtained adjustment and

correlation coefficients by the Taft and Catalan parameters. The dominant coefficient affecting the absorption and fluorescence bands of these picrate derivatives (**1**–**4**) is that describing the polarity/polarizability of the solvent ($C_{\pi^*}$ or $C_{SPP}^{N}$) having a positive value, corroborating the above-mentioned solvatochromic shifts with the solvent polarity. The coefficient controlling the H-donor capacity or acidity of the solvent, $C_\alpha$ or $C_{SA}$, has the negative values (Table 3), suggesting that the absorption and fluorescence bands shifted to lower energies with the increasing acidity of the solvent. This effect can be interpreted in terms of the stabilization of the resonance structures of the chromophore (Fig. 8). Though in all the resonance structures (a–c) having the positive charge located at the nitrogen atom, the structure "c" is in *p*-quinanoid form and it will be stabilized in acidic

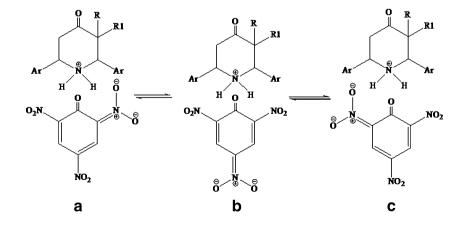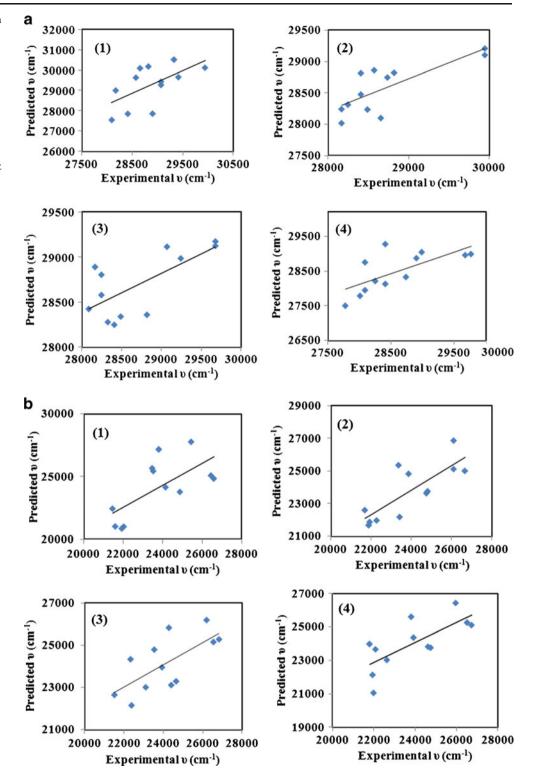**Fig. 8** Resonance structures of the picrate chromophore

**Fig. 9 a** Correlation between the experimental absorption wavenumber with the predicted values obtained by a multicomponent linear regression using the π*, α and β-scale (Taft) solvent parameters for **1–4**. **b** Correlation between the experimental fluorescence wavenumber with the predicted values obtained by a multicomponent linear regression using the π*, α and β-scale (Taft) solvent parameters for **1–4**



solvents because this resonance structure is predominant in the $S_1$ state, and the stabilization of the $S_1$ state with the solvent acidity would be more important than that of the $S_0$ state. Consequently, the energy gap between the $S_1$ and $S_0$ states decreases and the absorption and fluorescence wave-lengths shifted to longer wavelength with increasing solvent acidity. The adjusted coefficient representing the electron releasing ability or basicity of the solvent ($C_\beta$ or $C_{SB}$) values suggesting that the solvent basicity does not play an important role in absorption and fluorescence displacements.

**Table 3** Adjusted Coefficients (($\upsilon_x)_0$, $c_a$, $c_b$ and $c_c$) and Correlation Coefficients (r) for the Multilinear Regression Analysis of the Absorption $\upsilon_{ab}$ and Fluorescence $\upsilon_{fl}$ Wavenumbers and Stokes Shift ($\Delta\upsilon_{ss}$) of the picrate derivative **1–4** with the Solvent Polarity/Polarizability, and the Acid and Base Capacity Using the Taft ($\pi^*$, $\alpha$ and $\beta$) and the Catalan (SPP$^N$, SA and SB) Scales

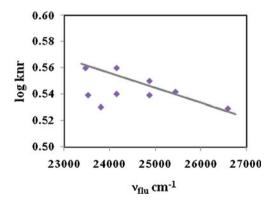| | ($\upsilon_x$) | ($\upsilon_x)_0$ cm$^{-1}$ | ($\pi^*$) | $c_\alpha$ | $c_\beta$ | r |
|---|---|---|---|---|---|---|
| **1** | $\lambda_{ab}$ | $(2.94\pm0.015)\times10^4$ | $(6.51\pm31.14)\times10^3$ | $(54.50\pm1.152)\times10^3$ | $(5.90\pm7.879)\times10^3$ | 0.89 |
| | $\lambda_{fl}$ | $(2.52\pm0.063)\times10^4$ | $(5.84\pm13.50)\times10^3$ | $-(22.71\pm43.347)\times10^3$ | $(24.15\pm30.642)\times10^3$ | 0.80 |
| | $\Delta\upsilon_{ss}=\upsilon_{ab}-\upsilon_{fl}$ | $(0.42\pm0.056)\times10^4$ | $(6.70\pm11.82)\times10^3$ | $-(17.255\pm38.555)\times10^3$ | $-(18.24\pm29.9231)\times10^3$ | 0.61 |
| | ($\upsilon_x$) | ($\upsilon_x)_0$ cm$^{-1}$ | $c_{SPP}^N$ | $c_{SA}$ | $c_{SB}$ | r |
| | $\lambda_{ab}$ | $(2.90\pm0.020)\times10^4$ | $(14.65\pm94.48)\times10^3$ | $-(12.420\pm40.389)\times10^3$ | $(12.29\pm42.232)\times10^3$ | 0.82 |
| | $\lambda_{fl}$ | $(2.46\pm0.070)\times10^4$ | $(31.22\pm32.89)\times10^3$ | $(115.21\pm1.405)\times10^3$ | $-(118.74\pm1.469)\times10^3$ | 0.78 |
| | $\Delta\upsilon_{ss}=\upsilon_{ab}-\upsilon_{fl}$ | $(0.44\pm0.055)\times10^4$ | $(32.68\pm25.75)\times10^3$ | $-(127.63\pm1.099)\times10^3$ | $(13.10\pm1.150)\times10^3$ | 0.73 |
| **2** | ($\upsilon_x$) | ($\upsilon_x)_0$ cm$^{-1}$ | ($\pi^*$) | $c_\alpha$ | $c_\beta$ | r |
| | $\lambda_{ab}$ | $(2.92\pm0.021)\times10^4$ | $(37.03\pm45.96)\times10^3$ | $-(43.81\pm1.498)\times10^3$ | $-(1.35\pm11.629)\times10^3$ | 0.82 |
| | $\lambda_{fl}$ | $(2.54\pm0.060)\times10^4$ | $(56.19\pm12.72)\times10^3$ | $-(69.33\pm4.147)\times10^3$ | $(12.51\pm3.218)\times10^3$ | 0.79 |
| | $\Delta\upsilon_{ss}=\upsilon_{ab}-\upsilon_{fl}$ | $(0.382\pm0.054)\times10^4$ | $(19.16\pm11.57)\times10^3$ | $(11.31\pm3.773)\times10^3$ | $-(13.86\pm2.928)\times10^3$ | 0.69 |
| | ($\upsilon_x$) | ($\upsilon_x)_0$ cm$^{-1}$ | $c_{SPP}^N$ | $c_{SA}$ | $c_{SB}$ | r |
| | $\lambda_{ab}$ | $(2.89\pm0.026)\times10^4$ | $(72.72\pm11.95)\times10^3$ | $-(23.85\pm5.103)\times10^3$ | $-(23.20\pm53.413)\times10^3$ | 0.80 |
| | $\lambda_{fl}$ | $(2.47\pm0.070)\times10^4$ | $(33.51\pm32.80)\times10^3$ | $-(126.05\pm1.402)\times10^3$ | $-(129.58\pm14.659)\times10^3$ | 0.72 |
| | $\Delta\upsilon_{ss}=\upsilon_{ab}-\upsilon_{fl}$ | $(0.42\pm0.057)\times10^4$ | $(26.30\pm26.50)\times10^3$ | $-(102.19\pm1.135)\times10^3$ | $(106.38\pm11.870)\times10^3$ | 0.70 |
| **3** | ($\upsilon_x$) | ($\upsilon_x)_0$ cm$^{-1}$ | ($\pi^*$) | $c_\alpha$ | $c_\beta$ | r |
| | $\lambda_{ab}$ | $(29.76\pm0.022)\times10^4$ | $-(2.18\pm17.57)\times10^3$ | $-(10.69\pm6.610)\times10^3$ | $(11.89\pm5.779)\times10^3$ | 0.80 |
| | $\lambda_{fl}$ | $(26.28\pm1.053)\times10^4$ | $-(63.41\pm85.70)\times10^3$ | $-(4.071\pm32.228)\times10^3$ | $(10.25\pm2.817)\times10^3$ | 0.69 |
| | $\Delta\upsilon_{ss}=\upsilon_{ab}-\upsilon_{fl}$ | $(3.473\pm1.026)\times10^4$ | $(61.23\pm83.53)\times10^3$ | $-(6.625\pm31.414)\times10^3$ | $(1.64\pm27.463)\times10^3$ | 0.64 |
| | ($\upsilon_x$) | ($\upsilon_x)_0$ cm$^{-1}$ | $c_{SPP}^N$ | $c_{SA}$ | $c_{SB}$ | r |
| | $\lambda_{ab}$ | $(26.27\pm0.089)\times10^4$ | $(253.43\pm101.86)\times10^3$ | $-(50.59\pm23.721)\times10^3$ | $(28.00\pm15.159)\times10^3$ | 0.69 |
| | $\lambda_{fl}$ | $(18.75\pm2.638)\times10^4$ | $(599.04\pm302.00)\times10^3$ | $-(115.78\pm70.328)\times10^3$ | $(60.24\pm44.944)\times10^3$ | 0.72 |
| | $\Delta\upsilon_{ss}=\upsilon_{ab}-\upsilon_{fl}$ | $(7.52\pm2.721)\times10^4$ | $-(345.60\pm311.42)\times10^3$ | $-(65.19\pm72.52)\times10^3$ | $-(32.24\pm46.346)\times10^3$ | 0.63 |
| **4** | ($\upsilon_x$) | ($\upsilon_x)_0$ cm$^{-1}$ | ($\pi^*$) | $c_\alpha$ | $c_\beta$ | r |
| | $\lambda_{ab}$ | $(29.21\pm0.173)\times10^4$ | $(61.50\pm36.62)\times10^3$ | $-(10.43\pm11.94)\times10^3$ | $-(5.27\pm9.266)\times10^3$ | 0.73 |
| | $\lambda_{fl}$ | $(25.52\pm0.565)\times10^4$ | $-(45.68\pm11.89)\times10^3$ | $-(13.05\pm38.27)\times10^3$ | $(17.99\pm3.009)\times10^3$ | 0.66 |
| | $\Delta\upsilon_{ss}=\upsilon_{ab}-\upsilon_{fl}$ | $(3.69\pm0.514)\times10^4$ | $-(15.82\pm10.28)\times10^3$ | $-(23.48\pm35.29)\times10^3$ | $(23.259\pm2.139)\times10^3$ | 0.69 |
| | ($\upsilon_x$) | ($\upsilon_x)_0$ cm$^{-1}$ | $c_{SPP}^N$ | $c_{SA}$ | $c_{SB}$ | r |
| | $\lambda_{ab}$ | $(28.78\pm0.274)\times10^4$ | $-(37.14\pm12.23)\times10^3$ | $-(8.28\pm54.831)\times10^3$ | $-(6.71\pm57.332)\times10^3$ | 0.72 |
| | $\lambda_{fl}$ | $(24.68\pm0.747)\times10^4$ | $(270.50\pm349.23)\times10^3$ | $-(66.45\pm149.284)\times10^3$ | $(97.95\pm156.093)\times10^3$ | 0.62 |
| | $\Delta\upsilon_{ss}=\upsilon_{ab}-\upsilon_{fl}$ | $(4.11\pm0.567)\times10^4$ | $(23.36\pm265.02)\times10^3$ | $-(88.18\pm113.286)\times10^3$ | $(91.24\pm11.845)\times10^3$ | 0.69 |



**Fig. 10** Correlation between the rate constant of non-radiative deactivation (log $k_{nr}$) with the fluorescence wavenumbers ($\upsilon_{flu}$ cm$^{-1}$) of **1** in several solvents

However, the fluorescence quantum yield and the lifetime values of these picrate derivatives (**1–4**) have been measured in common solvents. The solvent also affects the fluorescence quantum yield and lifetime of picrate derivatives and φ and τ values increase in polar/protic solvents (Table 1), although a general tendency in both parameters with respect to the solvent viscosity is not observed. These results indicate an extra non-radiative deactivation of these picrate derivatives, which is not governed by the solvent viscosity. Figure 10 shows a linear correlation between the $k_{nr}$ value and the fluorescence wave numbers of these picrate derivatives (**1–4**). It shows that the nature of the solvent have similar solvent parameter effect on these picrate derivatives [24].

It is well known that the flexibility/rigidity of the picrate derivatives can control the mechanics of internal conversion and it can be analyzed in terms of the planarity of the π-electron system [25]. This loss of planarity in the excited state implies a less rigid structure and the excitation energy is more easily converted to vibrational energy and dissipated as heat, enhancing the internal conversion processes. Drexhage et al., [26] pointed out that the structure loosens up upon excitation and enhancing the non-radiative deactivation processes. In these picrate derivatives (**1**–**4**), the presence of increased electrostatic interaction between the N-protonated piperidone ring and the picryl anion ring so that the picryl anion ring lies perpendicular to the plane of the piperidone ring i.e., non-coplanarity. Such a distortion from planarity leads to the non-radiative deactivation. Pavlopoulos et al., [3] also referred to the non-planarity of the chromophore provided by bulky substituents to explain the low fluorescence quantum yield.

The present photophysical characteristics of these picrate derivatives (**1**–**4**) would suggest a lower optical efficiency because of its lower fluorescence quantum yield. However, high optical densities are required to produce signals and under these conditions, the losses at the resonator cavity by the reabsorption and reemission effects can be important. These picrate derivatives are characterized by a higher Stokes shift which would reduce the losses at the resonator cavity by reabsorption and reemission effects, governed by the overlap between the absorption and emission spectra. Therefore, the lower fluorescence quantum yield to some extent, be compensated by its higher Stokes shift and high optic efficiencies for these picrate derivatives [27]. Because the higher Stokes shift and highest fluorescence quantum yield of the picrate derivatives are recommended to achieve the highest optic efficiencies in liquid media.

## Conclusions

The presence of increased electrostatic interaction between the N-protonated piperidone ring and picryl anion ring, makes the picrate anion ring lie perpendicular to the plane of the piperidone ring i.e., non-coplanarity. The picrate chromophore core originates a distortion from planarity in the picrate units, mainly in the excited state, which leads to an increase in the rate constant of non-radiative deactivation and in the Stokes shift. Both photophysical factors have an opposite effect on the optic efficiency. Thus, the increase in the loss of the resonator cavity due to the augmentation in the non-radiative processes could be compensated to some extent by a reduction in the reabsorption and reemission losses, owing to the high Stokes shift. From the photophysical studies, polar solvents are recommended to obtain the highest optic efficiencies in liquid media.

## References

1. Jayabharathi J, Manimekalai A, Consalata Vani T, Padmavathy M (2007) Synthesis, stereochemistry and antimicrobial evaluation of t(3)-benzyl-r(2), c(6)-diarylpiperidin-4-one and its derivatives. Eur J Med Chem 42:593–605
2. Shah M, Thangaraj K, Soong ML, Wolford LT, Boyer JH, Politzer IR, Pavlopoulos TG (1990) Pyrromethene-BF2 complexes as laser dyes: 1. Heteroat Chem 1:389–399
3. Pavlopoulos TG, Boyer JH, Thangaraj K, Sathyamoorthi G, Soong ML (1992) Laser dye spectroscopy of some pyrromethene-BF$_2$ complexes. Appl Opt 31:7089–7094
4. Lopez Arbeloa F, Ruiz Ojeda P, Lopez Arbeloa I (1988) On the aggregation of Rhodamine B in ethanol. Chem Phys Lett 148:253–258
5. Costela A, Moreno IG, Sastre R (2001) In Handbook of advanced electronic and photonic materials and devices; Nalwa HS (Ed) Academic Press: San Diego, CA, 7, 161
6. O'Neil MP (1993) Synchronously pumped visible laser dye with twice the efficiency of Rhodamine 6G. Opt Lett 18:37–38
7. Rhan MD, King TA (1995) Comparison of laser performance of dye molecules in sol-gel, polycom, ormosil, and poly(methyl methacrylate) host media. Appl Opt 34:8260–8271
8. Dubois A, Canva M, Brun A, Chaput F, Boilot JP (1996) Photostability of dye molecules trapped in solid matrices. Appl Opt 35:3193–3199
9. Yariv E, Schultheiss S, Saraidarov T, Reisfeld R (2001) Efficiency and photostability of dye doped solid state lasers in different hosts. Opt Mater 16:29–38
10. Lopez Arbeloa F, Lopez Arbeloa I, Lopez Arbeloa T (2001) In Handbook of advanced electronic and photonic materials and devices. Nalwa HS (Ed) Academic Press: C.A. San Diego, 7, 209
11. Manimekalai A, Jayabharathi J (2006) Protonation effect on chemical shifts of some piperidones – unusual influence by anions. Indian J Chem B 45:1686–1691
12. Guassian 03 program (2004) (Gaussian Inc., Wallingford CT)
13. Wilde AP, Watts RJ (1991) Solvent effects on metal-to-ligand charge-transfer bands in ortho-metalated complexes of iridium(III): estimates of transition dipole moments. J Phys Chem 95:622–629
14. Balamurali MM, Dogra SK (2004) Intra- and Intermolecular proton transfer in methyl-2-hydroxynicotinate. J Luminesc 110:147–163
15. Mazumdar S, Manoharan R, Dogra SK (1989) Solvatochromic effects in the fluorescence of a few diamino aromatic compounds. J Photochem Photobiol A 46:301–314
16. Hofer JE, Grabenstetter RJ, Wiig EO (1950) The fluorescence of cyanine and related dyes in the monomeric state. J Am Chem Soc 72:203–209
17. Assor Y, Burshtein Z, Rosenwaks S (1998) Spectroscopy and laser characteristics of copper-vapor-laser pumped pyrromethene-556 and pyrromethene-567 dye solutions. Appl Opt 37:4914–4920
18. Lopez Arbeloa I (1980) Fluorescence quantum yield evaluation. Reabsorption and reemission corrections. J Photochem 14:97–105
19. Bergstrom F, Mikhalyov I, Hagglof P, Wortmann R, Ny T, Johansson LBA (2002) Dimers of dipyrrometheneboron difluoride (BODIPY) with light spectroscopic applications in chemistry and biology. J Am Chem Soc 124:196–204
20. Marcus Y (1993) The properties of organic liquids that are relevant to their use as solvating solvents. Chem Soc Rev 22:409–416

21. Reichardt C (1994) Solvatochromic dyes as solvent polarity indicators. Chem Rev 94:2319–2358

22. Taft RW, Kamlet MJ (1976) The solvatochromic comparison method. 1. The $\beta$-scale of solvent hydrogen-bond acceptor (HBA) basicities. J Am Chem Soc 98:377–383

23. Catalan J, Diaz C, Lopez V, Perez P, de Paz y JLG, Rodriguez JG (1996) A generalized solvent basicity scale: the solvatochromism of 5-nitroindoline and its homomorph 1-methyl-5-nitroindoline. Liebigs Ann. 1785–1794

24. Eduardo C, Carvalho M, Brinn IM, Pinto AV, do Carmo M, Pinto FR (2000) Fluorescent symmetric phenazines from naphthoquinones: 3. Steady-state spectroscopy and solvent effect of seven phenazine derivatives: structure–photophysics correlations. J Photochem Photobiol A Chem 136:25–33

25. Birks JB (1970) Photophysics of aromatic molecules. Wiley-Interscience, London

26. Drexhage KH (1990) Dye lasers topics. In: Schafer FP (ed) Topics in applied physics, 1. Springer, Berlin, Germany, p 187

27. Allik T, Chandra S, Robinson TR, Hutchinson JA, Sathyamoorthi G, Boyer JH (1994) Laser performance and material properties of a high temperature plastic doped with pyrromethene-BF2 dyes. Mater Res Soc 329:291–296